Studies of a 96.9-nm laser in neutral cesium

C. P. J. Barty, G. Y. Yin, J. E. Field, D. A. King, K. H. Hahn, J. F. Young, and S. E. Harris

Edward L. Ginzton Laboratory, Stanford University, Stanford, California 94305

Investigations of a 96.9-nm laser in neutral cesium are described. Theoretical and experimental evidence is presented for the laser level designation and pumping mechanism. Measurements of the laser output are given, including saturated pulse energy, temporal profile, spatial profile, transition wavelength, gain cross section, and the variation of small signal gain with operating parameters. Comparisons of the temporal and spatial behavior of the 96.9-nm laser emission with respect to resonance line emission from ionic Cs are also presented.

I. INTRODUCTION

In 1988, gain and saturation of an extreme ultraviolet (XUV) laser at 96.9 nm in Cs vapor was reported [1]. This laser exhibited an extrapolated small signal gain of exp(83) and required less than 3 J of infrared pump energy. To the authors' knowledge, prior to this experiment, no conclusive evidence of Cs emission at 96.9 nm had been presented in the literature, nor did any theoretical supposition inferring gain at this wavelength exist. Subsequent spectroscopic evidence and atomic-physics calculations intimated that the upper laser level was embedded within the continuum of the first ion. Core-excited levels that are embedded within a continuum usually autoionize rapidly, making the accumulation of population difficult. But this need not be the case; work by Spong *et al.* [2,3] and Harris and Young [4] has shown, for example, that there are many levels in neutral Rb that have autoionization lifetimes exceeding 10 ps and several that exceed 100 ps. Such long lifetimes can result either from angular momentum and spin selection rules that, to first order, prohibit autoionization, or from fortuitous radial matrix-element cancellations. The possibility of using such levels to make extreme ultraviolet and soft-x-ray lasers has been noted by several workers [5–7]. The existence of inversion from an upper level embedded within a continuum has been inferred from fluorescence-intensity measurements by Silfvast and Wood [8].

Unlike previous laser-produced, plasma-excited, short-wavelength lasers [9,10], it was also deduced that this laser system was not directly pumped via photoionization, but was instead excited by hot electrons, which were the by-product of partial photoionization of the Cs vapor. While gain via this method had not been previously reported, the concept of photoelectron pumping was not without precedent. Wang and co-workers [11,12] used laser-produced-plasma soft x rays to create large densities of electrons in a Li and Ne mixture and consequently achieved populations of core-excited Li metastable states in excess of 10^{14} cm^{-3}. Electron excitation current densities created by this method can be on the order of 10^6 A/cm^2, much larger than conventional discharge tech-

nology. Recently, this pumping mechanism has been exploited to produce a saturated output at 116 nm in H$_2$ [13].

It should be noted that, since emission at 96.9 nm in Cs had not been reported in the literature, special attention was given to other possible origins of the laser emission, including transitions in higher ion stages of Cs. The relatively well-known spectroscopy [14–17] of Cs II and Cs III yields no transition at 96.9 nm. However, the wavelength of the Cs IV analog to the now well-studied 108.9-nm Xe III Auger laser [9,18–20] is not known and was considered as a possible source of the 96.9-nm emission. Clearly, a relatively large fraction of neutral Cs is ionized early in the pump pulse and thus could be photopumped by a latter portion of the pulse. The experimental and spectroscopic evidence presented here, however, does not support this hypothesis.

In this paper a summary of our theoretical and experimental investigations of the 96.9-nm Cs laser system is presented. Studies of the spectroscopy and atomic physics of neutral Cs illuminate several unique characteristics of the laser system. Experiments investigated the origin of the laser emission, the nature of the pumping mechanism, and the characteristics of the laser output. These experiments included measurements of the pulse energy, gain cross section, temporal and spatial profile, wavelength, and the variation of the small signal gain with respect to Cs pressure, pump energy, pump duration, and degree of traveling-wave excitation. In addition, comparisons of the temporal and spatial behavior of the 96.9-nm emission with respect to line emission from ionic Cs were conducted.

II. NEUTRAL Cs SPECTROSCOPY AND ATOMIC PHYSICS

From accurate measurement of the wavelength of the transition, reviews of published spectroscopy, and a series of atomic-physics calculations, much can be inferred about the neutral Cs XUV laser system. An energy-level diagram of the Cs 96.9-nm laser system is shown in Fig. 1. The 117 702 cm^{-1} energy of the upper level has been measured by vacuum ultraviolet (VUV) absorption spec-
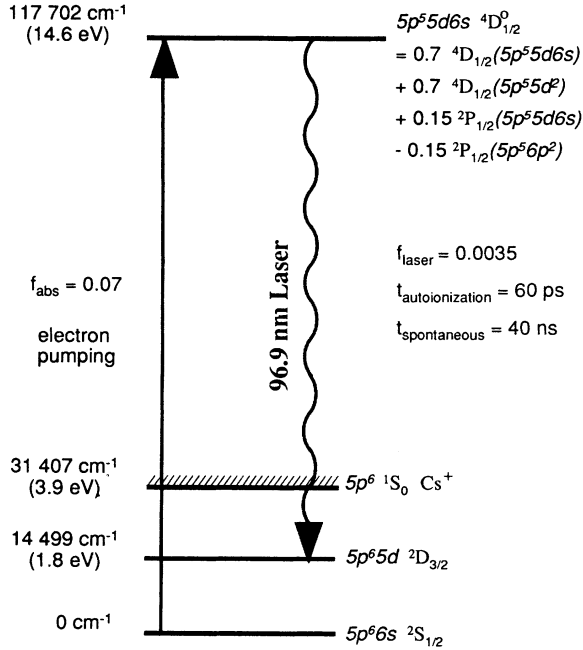

FIG. 1. Energy-level diagram of the 96.9-nm Cs I laser system.

troscopy [21,22], and the energy of the lower level is well known [22]. The difference of 96.897 nm agrees with two separate experimental measurements (which will be described later) that put the wavelength of this transition at 96.86±0.05 and 96.94±0.06 nm. The upper-level designation is obtained by matching an *ab initio* computer-generated, ground-sate, absorption spectra calculated with the RCN/RCG atomic-physics code developed by Cowan [23], with the known absorption spectra of Connerade [24] and the ejected-electron spectra of Pejcev and Ross [25].

The four largest components of the code-generated eigenvector expansion of the upper level are shown in Fig. 1. The two large quartet terms, arising from the $5d6s$ and $5d^2$ configurations, allow the level to have a relatively long autoionization lifetime, while the doublet terms allow for relatively large pumping and laser oscillator strengths. It is interesting to note that the combination of quartets which provide long lifetimes and doublets which provide the dipole-transition strength is qualitatively similar to a class of well-studied quartets in the alkali metals known as quasimetastables [4,26]. Spontaneous emission from quasimetastables can be very bright, almost one part in ten of the intensity of the ion resonance emission for the 109.1-nm Cs quasimetastable. In the case of quasimetastables, however, additional nonautoionizing doublet components reduce the oscillator strength from ground and thus make pumping difficult.

An obvious question arises as to whether the desired combination of good pumping oscillator strength, relatively long upper-state lifetime, and good laser oscillator strength is unique to the system depicted in Fig. 1. We have attempted to address this question by comparing the

predicted gains of all plausible transitions in neutral Cs. To do this we first tabulate the code-generated oscillator strengths from ground (f_{pump}), upper-level lifetimes (t), and laser-transition oscillator strengths (f_{laser}), of all transitions in the region around 100 nm. The same *ab initio* code run that is used in the level designation of Fig. 1 is used as a source for this tabulation. These values are then used to calculate a figure of merit (g_{FOM}), which is proportional to gain for each hypothetical lasing system. The figure of merit is the product of the gain cross section of the hypothetical lasing system and a function which is proportional to the peak inversion. The peak inversion is determined by maximizing the convolution integral of an assumed triangular-shaped pumping rate and an exponentially decaying upper-state population. The time constant of the exponential decay is determined by the combination of upper-level autoionization and spontaneous lifetimes. The functional form of the figure of merit is given by

$$g_{\text{FOM}} = \frac{f_{\text{pump}} f_{\text{laser}} \tau^3}{\Delta t} \times$$

$$\times \left\{ \left[1 - \exp\left[-\frac{t_p + \Delta t}{\tau} \right] \right] \right.$$

$$+ \frac{\tau}{\Delta t} \left[\left[\frac{\Delta t}{\tau} + 1 \right] \exp\left[-\frac{t_p + \Delta t}{\tau} \right] \right.$$

$$\left. - \left[\frac{t_p}{\tau} - 1 \right] - 2\exp\left[-\frac{t_p}{\tau} \right] \right] \right\} . \quad (1)$$

The time t_p in Eq. (1) is the the time at which the inversion is maximum and is given by

$$t_p = t \ln\left[2 - \exp\left[-\frac{\Delta t}{\tau} \right] \right] , \quad (2)$$

where Δt is the full width at half maximum (FWHM) of the triangular pumping pulse and τ is the combined decay rate of the upper level. The results of the calculations are given in Table I. We see clearly that one system has a figure of merit, and thus expected gain, that is an order of magnitude greater than its nearest rival and more than two orders of magnitude greater than all other systems. Completely independent of the previous comparisons with known spectroscopy, the highest-gain laser system is again the system depicted in Fig. 1. Besides providing additional verification of the original designation, Table I also suggests that only one core-excited laser should be easily seen or exhibit gain.

It should be noted that Eq. (1) has a strong dependence on the lifetime of the upper level. Since most autoionizing levels decay rapidly, it is assumed that the predominant broadening for each laser system in Table I is lifetime broadening. When combined with the pump-pulse convolution described previously, this assumption leads to a cubic dependence for the gain figure of merit with respect to upper-level lifetime. This assumption is most valid for short-lifetime systems. For 100-nm radiation in a Cs vapor, Doppler broadening becomes comparable to

TABLE I. Gain figure of merit for transitions in the vicinity of 100 nm in Cs I.

Code predicted values			
Upper level (1000 cm^{-1})	Lower level (1000 cm^{-1})	Wavelength (nm)	g_{FOM}
114.0907 $^4D^\circ_{1/2}$	17.9574 $^2S_{1/2}$	104.02	0.000 000 7
114.0907 $^4D^\circ_{1/2}$	13.4329 $^2D_{3/2}$	99.35	0.003 505 6
114.5559 $^4D^\circ_{3/2}$	17.9574 $^2S_{1/2}$	103.52	0.002 993 6
114.5559 $^4D^\circ_{3/2}$	13.4329 $^2D_{3/2}$	98.89	14.711 460 5
114.5559 $^4D^\circ_{3/2}$	13.5692 $^2D_{5/2}$	99.02	4.449 006 2
117.2184 $^2D^\circ_{3/2}$	17.9574 $^2S_{1/2}$	100.74	0.005 368 3
117.2184 $^2D^\circ_{3/2}$	13.4329 $^2D_{3/2}$	96.35	0.116 896 4
117.2184 $^2D^\circ_{3/2}$	13.5692 $^2D_{5/2}$	96.48	0.412 275 8
117.6329 $^4D^\circ_{1/2}$	17.9574 $^2S_{1/2}$	100.33	0.221 001 9
117.6329 $^4D^\circ_{1/2}$	13.4329 $^2D_{3/2}$	95.97	137.748 293 4
117.8634 $^2D^\circ_{3/2}$	17.9574 $^2S_{1/2}$	100.09	0.000 000 0
117.8634 $^2D^\circ_{3/2}$	13.4329 $^2D_{3/2}$	95.76	0.021 940 2
117.8634 $^2D^\circ_{3/2}$	13.5692 $^2D_{5/2}$	95.88	0.000 187 7
119.1902 $^4D^\circ_{3/2}$	17.9574 $^2S_{1/2}$	98.78	0.000 000 0
119.1902 $^4D^\circ_{3/2}$	13.4329 $^2D_{3/2}$	94.56	0.000 004 2
119.1902 $^4D^\circ_{3/2}$	13.5692 $^2D_{5/2}$	94.68	0.000 011 1
120.3515 $^4P^\circ_{3/2}$	17.9574 $^2S_{1/2}$	97.66	0.000 024 2
120.3515 $^4P^\circ_{3/2}$	13.4329 $^2D_{3/2}$	93.53	0.000 007 8
120.3515 $^4P^\circ_{3/2}$	13.5692 $^2D_{5/2}$	93.65	0.002 536 1
121.2800 $^4P^\circ_{1/2}$	17.9574 $^2S_{1/2}$	96.78	0.000 000 0
121.2800 $^4P^\circ_{1/2}$	13.4329 $^2D_{3/2}$	92.72	0.000 000 0
122.0955 $^2P^\circ_{3/2}$	17.9574 $^2S_{1/2}$	96.03	0.000 000 0
122.0955 $^2P^\circ_{3/2}$	13.4329 $^2D_{3/2}$	92.03	0.000 000 2
122.0955 $^2P^\circ_{3/2}$	13.5692 $^2D_{5/2}$	92.14	0.000 000 0

lifetime broadening when autoionization lifetimes exceed ~50 ps. For longer lifetimes, Eq. (1) must be modified and will result in a less rapid time dependence. It should also be noted that, because of large mixing between the $5d6s$ and $5d^2$ configurations, code predictions for the 96.9-nm laser autoionization lifetime can vary greatly. The 60-ps lifetime shown in Fig. 1 is approximately the median calculated lifetime of the level. Several different calculations were also performed in which the configuration average energies of the $5d6s$ and $5d^2$ configurations were independently adjusted, while all other scaling parameters remained constant. Lifetimes as short as 45 ps and as long as 150 ps were obtained. In all cases the same $^4D^\circ_{1/2}$ upper level remains the dominant core-excited laser system with respect to our figure-of-merit calculations.

Code predictions of transition oscillator strengths and spontaneous-emission rates are not dramatically affected by relative configuration placement. The calculated laser oscillator strength of 0.0035 implies a Doppler-broadened stimulated-emission cross section of 1.7×10^{-14} cm^2. The relatively long spontaneous-decay time of 40 ns implies a relatively low branching ratio to radiation of 0.0014. Therefore it should be difficult to observe spontaneous emission from this level. Emission at 96.9 nm may have been observed from a discharge in earlier work on quasimetastables [26]. We have recently learned of two separate high-resolution XUV measurements of neutral Cs at the National Institute of Standards and Technology (NIST). In these measurements each spectroscop-

ic plate reveals a very weak line at 96.9046 nm [27]. In addition, no line at or near 96.9 nm exists on other NIST plates taken for ionic Cs. In order to obtain a significant output at 96.9 nm, it is necessary for the upper level to be excited very rapidly and consequently have the stimulated-emission rate exceed the autoionization rate.

III. Cs EXPERIMENTAL ARRANGEMENTS

In our experiments rapid excitation is typically provided via an intense 15-ps, 1064-nm laser pulse. The pulse is focused by a cylindrical lens onto a target which resides within a Cs heat-pipe cell. At the surface of the target, a dense plasma is created. This plasma radiates incoherent soft x rays and in the process partially photoionizes the surrounding Cs vapor. The resulting photoelectrons may then collisionally excite the 96.9-nm laser transition. In order to achieve large single-pass gains with this excitation, it is necessary that the length of the line focus be several cm. However, the short autoionization lifetime of the upper level and the finite transit time of the 96.9-nm radiation through the gain region limit the useful length of the line focus unless a traveling-wave excitation is used.

A schematic of one of the synchronous traveling-wave excitation arrangements used in our studies is shown in Fig. 2. The geometry is a modification of that used by Sher et al. [20] for the Xe 108.9-nm Auger laser. A 2.5-J, 15-ps, 1064-nm pulse is incident upon a cylindrical lens at 65° from normal and is focused onto a target which is
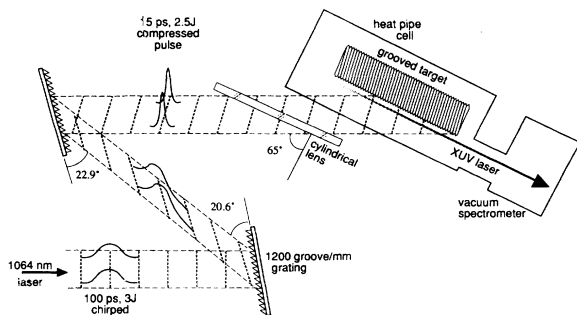
FIG. 2. Schematic of the short-pulse, grating-assisted, synchronous traveling-wave pumping geometry.

parallel to the lens. The large angle of incidence expands the length of illumination by $1/\cos(65°)=2.4$, producing a $17\ \text{cm}\times100\ \mu\text{m}$ line focus. By itself, this geometry would produce a plasma sweeping along the target at a speed of $c/\sin(65°)=1.1\times c$, resulting in a synchronism mismatch of 3.1 ps/cm of target length. In these experiments, however, the 15-ps long pulse is formed by chirping a mode-locked 1064-nm pulse in a fiber, amplifying it in Nd:YAG and Nd:glass stages, and compressing the resulting 120-ps pulse with a parallel-grating pair [28,29]. The second grating of this pair is tilted off true parallelism by 2.3° so as to produce a tilted wave front [30] that exactly compensates for the group-velocity lead of the oblique geometry. The result is a plasma and its associated pulse of soft x rays, which travels along the target at the speed of light. Variation of the traveling-wave speed can be accomplished by changing the angle of the last grating or by adding an additional grating after the compression pair. The full energy repetition rate for experiments was one shot every 5 min.

The heat-pipe target chamber was typically operated at a Cs density of $6.3\times10^{16}\ \text{cm}^{-3}$. The surface of the 304 stainless-steel target rod was grooved at a pitch of 43 per cm and, during the experiments, was wet with liquid Cs. Two separate heat-pipe chambers were designed and used. First, a 20-cm-target-length cell [1] was used to maximize the length of the line focus and thus the total single-pass gain of the system. With this cell and the given input-beam diameter, we could obtain a plasma length of 17 cm and easily saturate the laser transition. However, because of its design, this cell allowed radiation from a relatively large region ($\sim1\ \text{cm}^2$) in front of the target to be collected by our detection systems. In order to study more carefully the spectroscopy of the actual lasing volume, a smaller heat pipe was designed. Schematically, this cell is shown in Fig. 3. In this case the laser-produced plasma region was limited to a 5-cm length. Both normal- and 60°-incidence illumination of the target were possible. A heating and cooling block in thermal contact with the target allowed the formation of a liquid-Cs layer on the target to be controlled. A pair of vertical- and horizontal-slit apertures allowed the viewing volume to be selected with 100-μm resolution. A movable visible mirror plus an on-axis white-light source allowed the Cs pressure to be monitored as a function of distance from
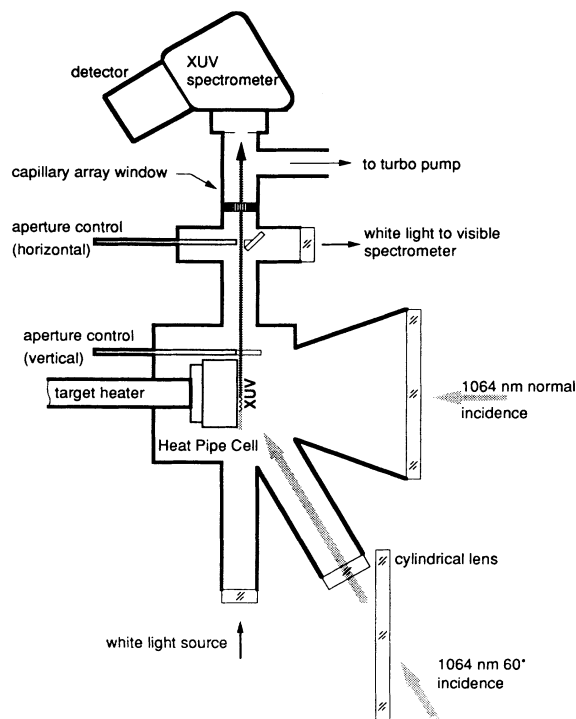
FIG. 3. Small-cell experimental arrangement.

target prior to each shot.

A variety of detection systems were used and will be described in conjunction with their associated experiments. Isolation of the detection systems from the He buffer gas of the heat-pipe cell was most often accomplished by differential pumping through a capillary array; however, in rare cases, a thin film of In was used as a vacuum window.

IV. Cs EXPERIMENTAL RESULTS
(20-cm CELL)

In all cases the small signal gain was determined by measuring the relative 96.9-nm energy as a function of plasma length for short sections of the target. In the 20-cm-cell experiments, the signal was monitored with a 1-m VUV spectrometer (McPherson model no. 225) equipped with a 600-ps-resolution stacked microchannel-plate detector. The length of the laser region was varied by masking the input plasma-producing beam. The gain was measured for several sections along the 17-cm target and was uniform, averaging 4.9 cm^{-1}. This yields a total extrapolated small signal gain of exp(83). A typical gain measurement is shown in Fig. 4. The solid line represents a computer-generated fit to a spectrally integrated superfluorescence formula [31]. Figure 5 shows the dependence of the laser-output energy for the entire plasma length. The linear increase after 4 cm clearly indicates saturation of the transition. In this case a 4-cm plasma length corresponds to only 400 mJ of pump energy on target. The 96.9-nm full-length energy of 1.5 μJ was measured by replacing the capillary-array-interfaced spectrometer and microchannel-plate detector with an In
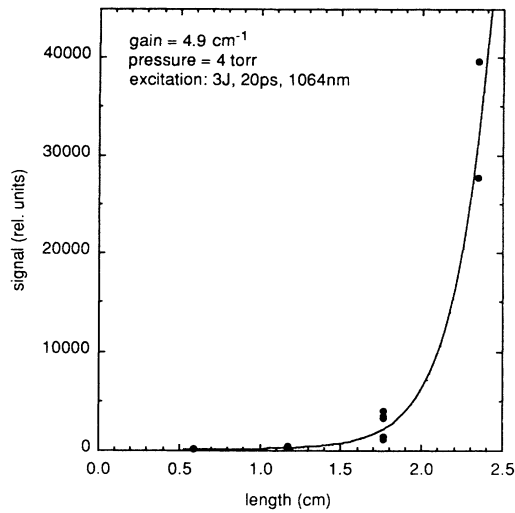
FIG. 4. 96.9-nm output vs length, small-signal-gain measurement for Cs I laser.

FIG. 6. Temporal profile of saturated 96.9-nm output.

filter and a calibrated Al vacuum photodiode.

The temporal profile of the full-length output is shown in Fig. 6. The measurement was made with a Kentec soft-x-ray streak camera, which was mounted in the exit plane of a 0.2-m VUV spectrometer (Acton model no. VM 502). Vacuum isolation was achieved with an In filter. The streak camera was equipped with a KBr-coated In photocathode. The steep leading edge of the pulse is indicative of a swept-gain amplifier and is qualitatively similar to the swept-gain output of the 108.9-nm Xe Auger laser [20]. It should be noted that the rising edge of the laser output appears to be faster than the resolution of the camera, which was ~20 ps. Combined with our energy measurement, the 32 ps FWHM shown in Fig. 6 yields a peak power of 4.7×10^5 W.

A crude estimate of the beam divergence of the laser output was made by placing a two-dimensional Vidicon detector (EG&G PARC model no. 1254) ~1 m from the

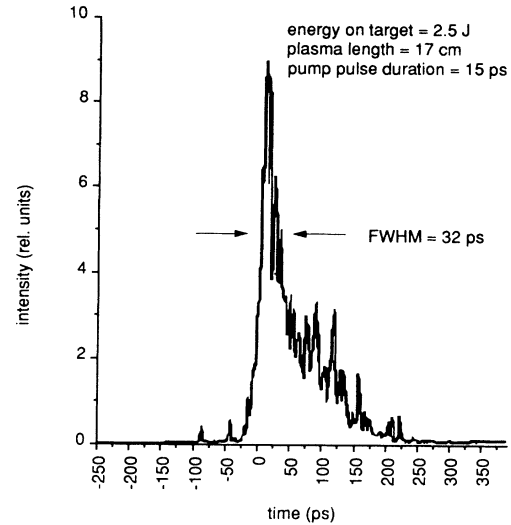end of the plasma. Again, an In filter was used for vacuum isolation. The output of the vidicon was monitored with an xyz oscilloscope. Although this method did not provide quantitative information in the z dimension, it did provide an upper bound of 4 mm in diameter for the beam cross-sectional area at the location of the detector. Combined with measurements of the lasing volume that will be described shortly, this cross-sectional area implies a beam divergence of <2 mrad. It should be noted that additional temporal and spatial measurements, which would have required the use of an In filter for vacuum isolation, were not performed because of fear of filter rupture and subsequent destruction of the detection systems.

The variation of the small signal gain with ambient Cs pressure and the variation of the small signal output with Cs pressure are shown in Figs. 7 and 8. Assuming no change in excitation dynamics, these curves imply that the ambient Cs absorption cross section at 96.9 nm is
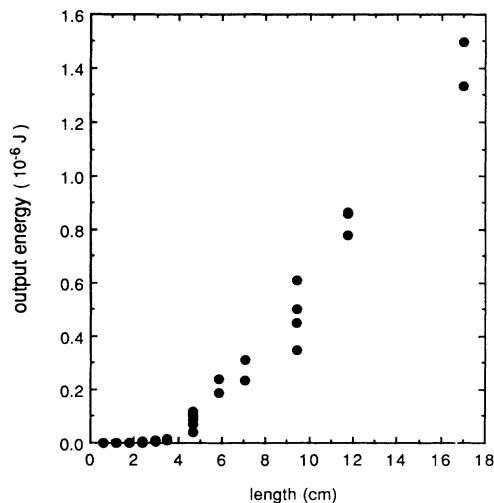

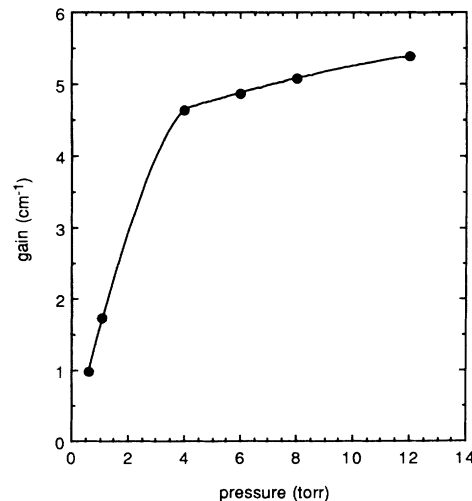FIG. 5. 96.9-nm energy vs length for long plasma lengths.

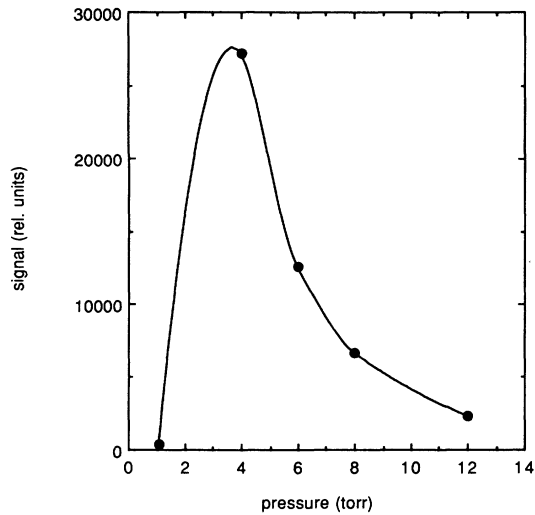FIG. 7. Gain vs pressure for the 96.9-nm Cs laser.

FIG. 8. 96.9-nm output vs pressure for 2-cm target illumination.

0.3×10^{-18} cm^2. This agrees qualitatively with the VUV absorption spectra of Connerade [24], which shows a feature at around 96.9 nm. Reliable measurements at pressures much below 1 Torr are difficult because of rapidly changing target conditions; in particular, it is difficult to maintain a liquid-Cs coating of the target at low pressures. Under these conditions the composition of the laser-produced plasma is dramatically altered from a relatively high-z species Cs to a lower-z species Fe. While use of a stainless-steel target does not cause lasing to cease, it does yield a significantly lower gain.

Several experiments were performed to test the importance of synchronous traveling-wave pumping. The second grating angle and target angle of incidence were changed to produce a group-velocity lead to 10 ps per cm of target length or a traveling-wave speed $v = 1.43c$. At a constant pump intensity on a target of 9×10^{11} W/cm^2, the output signal for a 2.4-cm plasma length was reduced by a factor of 525 and the gain was reduced to 1.8 cm^{-1}. In general, the group velocity in an inverted media for a pulse on line center is slower than the speed of light in vacuum [21], and therefore the optimum traveling-wave speed may actually be slower than the vacuum speed of light. To confirm this supposition, the last turning mirror before our cylindrical lens was replaced by another grating. The angle of this grating was chosen so that the excitation speed across the target was now $v = 0.34c$. At an intensity of 8×10^{11} W/cm^2 on target, this arrangement produced a gain of 4.3 cm^{-1}. Clearly, the correct choice of traveling-wave speed is essential for producing the highest gain. No attempt to optimize the gain as a function of traveling-wave velocity was made. In order to make an accurate prediction of the optimum speed, one would need more precise knowledge of the linewidth of the transition under the experimental conditions.

Using synchronous pumping ($v = c$), the small signal gain for different pump-pulse durations was compared. The results for 15-ps and 190-ps excitation are depicted

in Fig. 9. The energy on target was held constant. The signal levels of the 90.1-nm Cs II and 63.8-nm Cs III resonance lines were unchanged, indicating that the reduction in gain should not be directly attributed to reduced soft-x-ray conversion, but is more likely due to the short lifetime of the lasing transition. A gain of 1.0 cm^{-1} was also measured for an input-pulse duration of 1100 ps and approximately the same pulse energy. However, other studies [32] indicate that the x-ray flux was very likely lower in this case.

Finally, an accurate measurement of the wavelength of the transition was attempted. Because spontaneous emission at the laser wavelength was very difficult to detect, the full-length output of the 96.9-nm laser was used. In order to avoid aliasing effects due to the directional nature of the laser output, the beam was reflected off of a double scatterer before entering the 1.0-m normal-incidence spectrometer. This scatterer consisted of two ground-glass plates oriented parallel to one another and at $\sim 45°$ with respect to the incident-beam propagation axis. The spectrometer was equipped with a 1200-groove/mm grating and was scanned by 0.025 nm per shot to record the spectral profile. Approximately 50 shots were taken to determine the peak of the profile. Absolute calibration was made using the same technique and the same length emission from the Xe 108.9-nm Auger laser. Assuming linearity of the spectrometer step size, the Cs laser wavelength was determined to be 96.86 ± 0.05 nm.

V. Cs EXPERIMENTAL RESULTS (5-cm CELL)

More complete spectra measurements were made with the 5-cm-cell arrangement. Using a gated multichannel detector, radiation from various ion stages was monitored on a single-shot basis. A schematic of the multichannel XUV detection system is shown in Fig. 10 and consisted
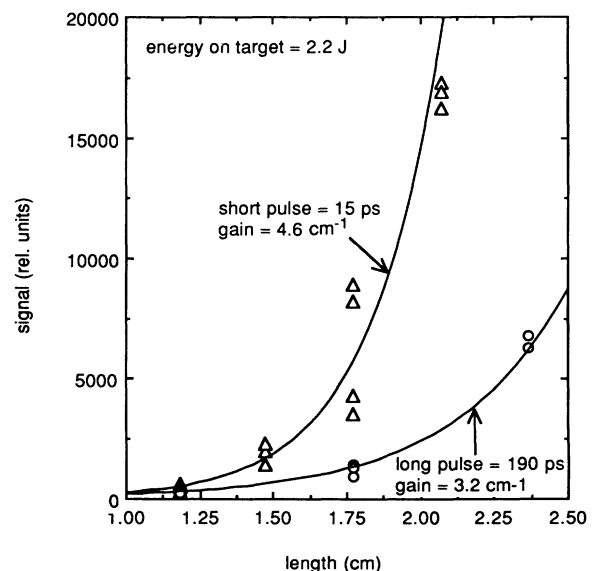

FIG. 9. Signal vs length-gain measurements for long- and short-pulse excitation.
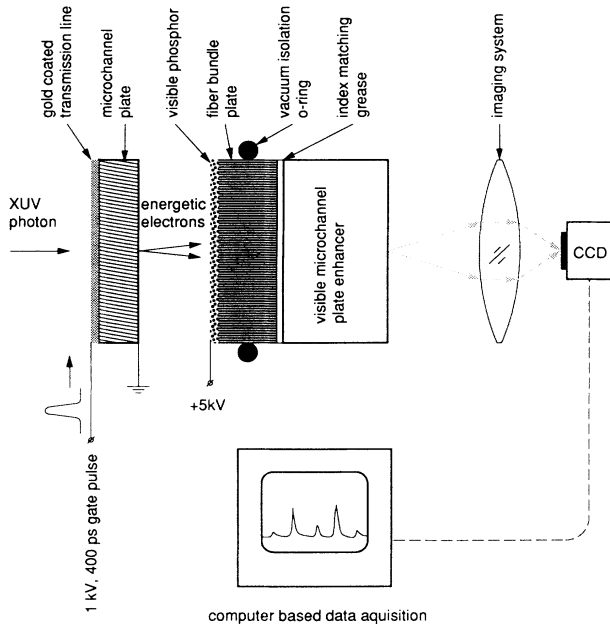
FIG. 10. Gated XUV detection system.

FIG. 12. Gated spectra vs length at peak 96.8-nm emission time (full scale).

of a cesium-iodide-coated, gated (400 ps FWHM) microchannel plate whose output electrons were electrostatically imaged onto a visible phosphor [33,34]. The phosphor was coated on a fiber-optic bundle, which provided vacuum isolation. A visible microchannel-plate enhancer was contact coupled to the fiber bundle, and single-shot data were collected by imaging the visible-enhancer output with a charge-coupled-device (CCD) camera (Photometrics). By varying the voltages of the phosphor and visible enhancer, a 10^5 dynamic range could be achieved. Thus gain measurements over a large spectral range could be obtained simultaneously. A temporal resolution of 250 ps was obtained by adjusting the timing of the gate pulse to the cesium-iodide-coated microchannel plate.
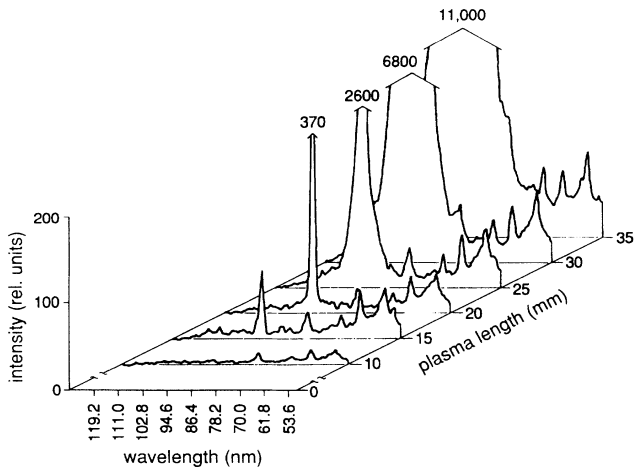
With this system placed in the image plane of a 0.2-m spectrometer (Acton model no. VM 502), a 120-nm-wide spectrum could be viewed in a single shot. Spectra as a function of plasma length are depicted in Figs. 11 and 12. Note that the emission at 96.9 nm completely dominates for lengths longer than 25 mm. The large pedestal on long-length spectra is due to cross talk between channels in the visible enhancer. Also note the absence of 96.9-nm emission at 10 mm of plasma length. This threshold behavior is further illustrated in Fig. 13. In this case a 5-cm plasma was used and the input-pulse energy was at-

FIG. 11. Gated spectra vs length at peak 96.9-nm emission time (reduced scale).
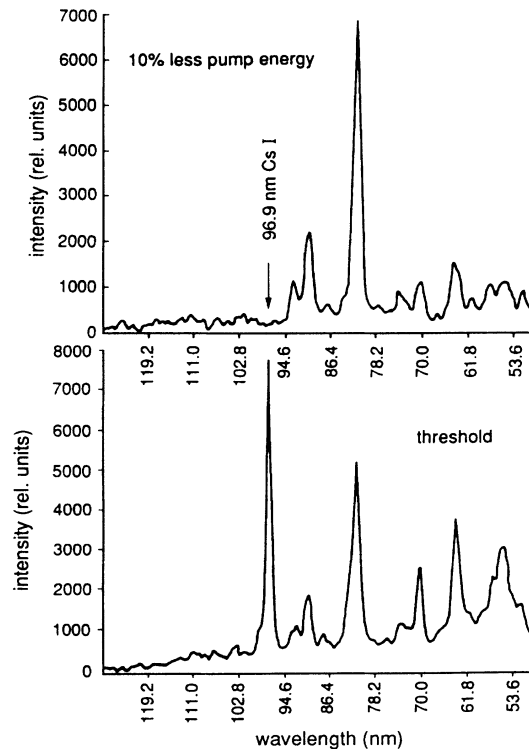

FIG. 13. Threshold behavior of 96.9-nm Cs laser output for 10% change in pump-pulse energy.

tenuated until the emission at 96.9 nm was on scale with that of the Cs II resonance line at 81.4 nm. With 10% further attenuation of the pump-laser energy, the signal at 96.9 nm completely disappears, whereas the ion emission from Cs II, Cs III, and Cs IV remains relatively unchanged.

A quantitative study of the lasing volume under the above conditions was also conducted. Because of the large signal at peak timing, the spatial profile of the gain region could be obtained by scanning a micrometer-controlled 200-μm slit downstream from the target. The vertical profile was taken with the slit oriented in the plane of the input beam and placed in contact with the end of the cylindrical target. The horizontal profile was taken with the slit oriented perpendicular to the plane of incidence of the pump beam. Because of the geometry of the cell, this slit resided 22 cm from the end of the target. For comparison, scans of emission from both the 96.9-nm Cs and 108.9-nm Xe lasers were performed. The normalized results of these scans are shown in Figs. 14 and 15. The emission in the Cs case emanates from a much smaller volume. From Figs. 14 and 15, the cross-sectional area of the emission volume was estimated to be $\sim 200 \times 125$ μm^2.

In order to obtain higher resolution, the multichannel XUV detection system was placed in the image plane of the 1-m normal-incidence spectrometer (McPherson model no. 225). This resulted in a resolution of 0.0284 nm/pixel for our 560-pixel-wide CCD array. By using a 3-cm normal-incidence line focus and summing several shots, a large signal-to-noise ratio was obtained. Under these conditions the gain at 96.9 nm was reduced to a level that did not obscure other line emission. A typical spectra is shown in Fig. 16. By using the strong Cs IV emission at 98.61 nm and the Cs II emission at 90.127 nm for calibration, this spectra places the Cs laser wavelength at 96.94±0.06 nm.
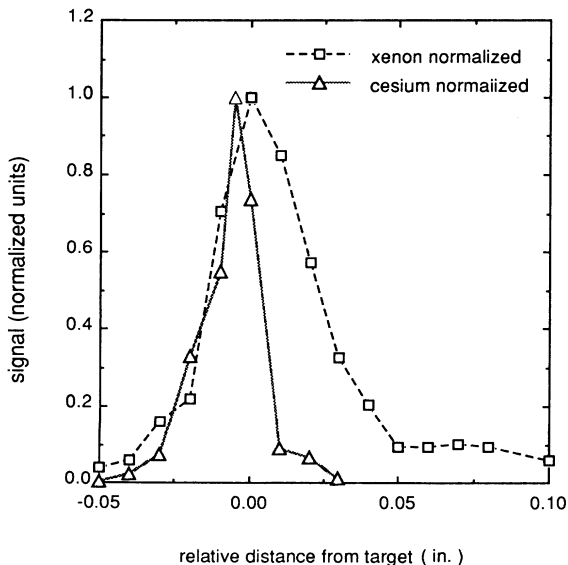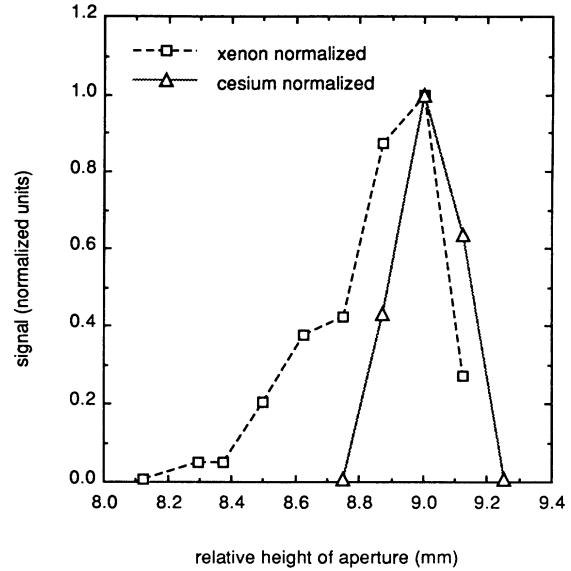

FIG. 15. Normalized vertical profile of emission volumes for the 96.9-nm Cs laser and 108.9-nm Xe III laser.

In order to accumulate more rapidly spectra of approximately the same line-to-line contrast and signal-to-noise ratio, the Nd:glass amplifiers of the pump laser were bypassed and an additional 12-mm-diam Nd:YAG amplifier was used to produce a 350-mJ, 300-ps, 2-Hz, 1064-nm pumping source. When used at 60° incidence, i.e., $v = 1.15c$ traveling wave, this arrangement allowed the accumulation of one complete spectra in ~ 2 min versus the ~ 60 min required in Fig. 16.

By using a micrometer-controlled stainless-steel block located adjacent to the target rod, low-level emission for regions above and below the line focus could be selectively obscured. In this way the spatial variation of 96.9-nm

FIG. 14. Normalized horizontal profile of emission volumes for the 96.9-nm Cs laser and 108.9-nm Xe III laser.
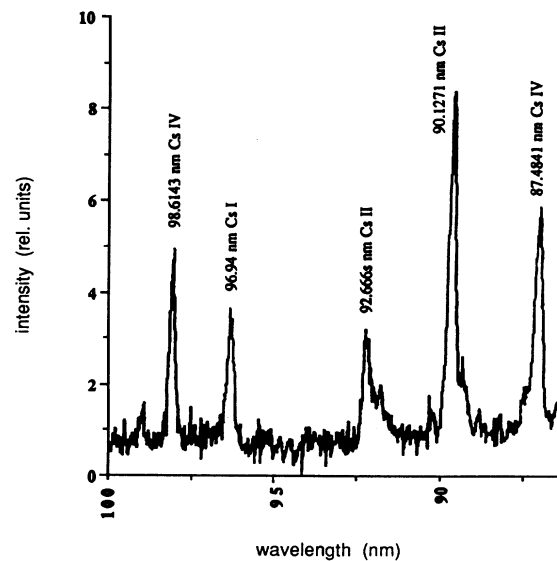

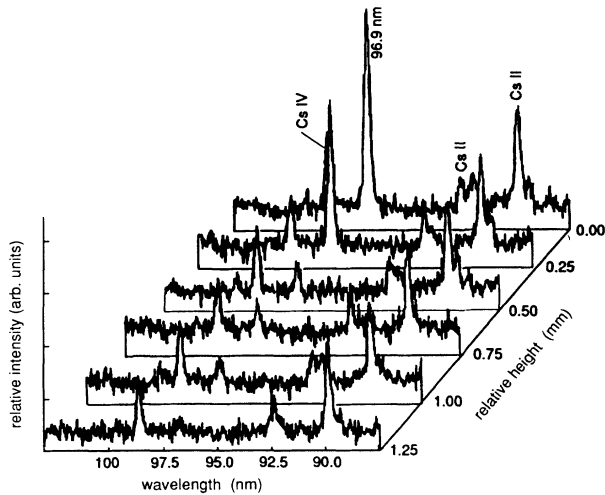FIG. 16. High-resolution gated Cs spectra.

FIG. 17. Spatial variation of 96.9-nm emission with respect to Cs-ion line emission.

emission with respect to other line emission could be studied. A representation of the spectra obtained as the block was raised from below the line focus to slightly above it is given in Fig. 17. From this figure it is clear that emissions due to transitions in ionic Cs originate from a much larger region than that of the 96.9-nm laser.

The timing of the 96.9-nm emission with respect to ion line radiation was also monitored. Possible differences in transit time through the gain region were avoided by using a high-intensity spot focus of $\sim 10^{12}$ W/cm^2 on target. The timing of the microchannel-plate gate was stepped in 250-ps increments. The result is shown in Fig. 18. In this figure it appears that emission at 96.9 nm occurs at least 250 ps late with respect to the Cs II lines at 92.6 and 90.1 nm. It should be noted that these Cs II lines are the result of direct soft-x-ray photoionization of the 5p subshell in Cs. The delay of emission at 96.9 nm is consistent with a system which is not pumped directly by plasma soft x rays, but is instead pumped indirectly by photoionization-created electrons.
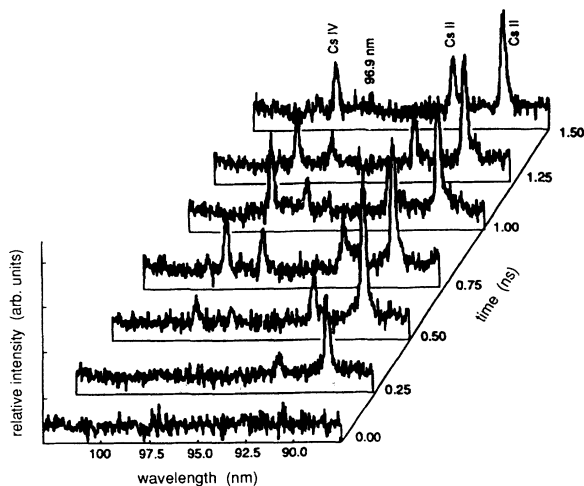

FIG. 18. Temporal variation of 96.9-nm emission with respect to Cs-ion line emission.

VI. DISCUSSION OF RESULTS

The measured gains are consistent with simple estimates based on photoelectron pumping. For example, with a 1064-nm power density on a target of 1.5×10^{12} W/cm^2 and assuming that only 3% of the 1064-nm laser energy is converted to soft x rays, the resulting laser-produced plasma may be modeled as a blackbody radiator with an effective temperature of 25 eV. Because of the large 5p and 4d photoionization cross sections [35] of Cs at a distance of 0.5 mm from the target, this blackbody will create a photoelectron density of approximately 2×10^{16} cm^{-3} with a Maxwell-Boltzmann-like temperature of ~ 30 eV. At this temperature, calculations with the RCN/RCG code yield a temperature-averaged electron excitation cross section times velocity product for the upper laser level of 3.5×10^9 cm^3/s. Using the median autoionization lifetime of 62 ps as the effective pumping time yields an upper-level population density of 2.8×10^{14} cm^{-3}. This upper-level population times the calculated gain cross section of 1.7×10^{-14} cm^2 gives a gain coefficient of 4.8 cm^{-1} as compared with our measured value of 4.9 cm^{-1}. It should be noted that this calculation assumes that the lower laser level is empty. Under the above conditions, a simple multilevel rate-equation model of electron pumping into and out of the lower laser level predicts that the laser system is not inverted. However, both of these calculations are strongly dependent upon the accuracy of code-generated electron excitation rates, autoionization lifetimes, and valence-level lifetimes. The predicted noninversion is not significant in comparison to the accumulated error that is associated with the use of these computer-generated parameters. We believe that the timing evidence indicates that the lower level is not laser dumped, and we do not now believe that the atomic physics supports the possibility of lasing without inversion [36], as was previously suggested [1].

Independent of calculated autoionization times or assumptions of laser to x-ray conversion, we may also use our measured data to estimate the gain cross section of the lasing transition. From Figs. 5, 14, and 15, we see that the saturated lasing volume is 13 cm $\times$ 0.0125 cm $\times$ 0.02 cm = 0.003 25 cm^3. The ratio of the measured saturated output energy (1.5 μJ) to this volume gives the photon density. For a fully saturated transition, this photon density is equivalent to the inversion density N^*. The gain cross section (σ) is then just the ratio of the measured small signal gain (4.9 cm^{-1}) and N^*. The result is an experimentally determined gain cross section of 2.2×10^{-14} cm^2 as compared with the code-calculated, Doppler-broadened gain cross section of 1.7×10^{-14} cm^2. This calculation involves only the transition oscillator strength, which is subject to far less variation from configuration mixing than code calculations of autoionization lifetimes. It should also be noted that the measured and predicted cross sections are both relatively small. Strong transitions between bound levels in doubly ionized species, such as the 108.9-nm Xe III Auger laser, have cross sections that are typically an order of magnitude larger.

VII. CONCLUSIONS

The Cs 96.9-nm laser is an extremely high-gain system exp(83) with remarkably low-pump-energy requirements of < 3 J. Since this laser was not predicted, the origin of the laser transition has been a matter of debate. We believe that the laser transition occurs in neutral Cs and is one in which the upper level is embedded within a continuum. This conclusion is based upon several factors. These include comparison of known and calculated spectra, good agreement of the measured wavelength with a line seen in NIST high-resolution neutral Cs studies, the unique temporal and spatial characteristics of the laser emission with respect to ion line emission, an independent figure-of-merit calculation that suggests that the 96.9-nm laser system is the strongest possible neutral laser and finally, general agreement between measured quantities and predictions of the gain and gain cross section. In addition to the above evidence, which supports the assumption of a neutral lasing species, the following arguments can be made against an assumption that emission arises from an ionic transition. The same NIST studies that show lines at 96.9 nm in neutral Cs do not exhibit lines at this wavelength for higher ion stages of Cs [27]. The lack of ion emission is very strong but not conclusive evidence, since the spark-gap excitation employed in the NIST studies is not the same as the soft-x-ray excitation used here. Independent of the NIST result, the spectroscopy of Cs II and Cs III is well known [14–17] and also does not support a transition at 96.9 nm. The spectroscopy of Cs IV has not been published beyond the resonance lines [37]. In particular, the wavelength of the Cs IV analog to the Xe III 108.9-nm Auger laser is not known. RCN/RCG calculations put this wavelength somewhat close at around 94 nm. Code-generated transition wavelengths are subject to approximately 10% accuracy. A code calculation of the oscillator strength, which is generally more accurate, yields a gain cross section for a Xe III–like Cs IV laser which is about an order of magnitude larger than that determined experimentally. Finally, the possibility of lasing from an even higher ion stage would require a very convoluted and inefficient pumping route consisting of multiple ionizations and excitations.

Timing evidence with respect to Cs-ion line emission and the agreement of measured gains with calculations suggest that the 96.9-nm Cs laser is electron pumped. At electron densities of 2×10^{16} cm^{-3} and electron temperatures of 30 eV, the photoionization-created electron source is equivalent to a discharge with a current density of nearly $eN_e v_e = 10^6$ A/cm^2 and a rise time on scale with the pump-laser pulse. This extremely large current density suggests that conventional discharge laser systems also may be operated with this compact experimental arrangement. Recently, Benerofe et al. [13] have employed this technique to saturate a number of well-known VUV transitions in molecular hydrogen.

The existence of a core-excited neutral Cs laser does not necessarily imply that an analogous system will exist in lighter alkali metals or an isoelectronic ion. This is especially true in light of the unique role that configuration mixing plays in determining the characteristics of the Cs laser transition. In particular, the Cs laser system simultaneously has a large pumping oscillator strength, a relatively long autoionization lifetime, and good laser oscillator strength. From simple dipole arguments, one would expect that systems possessing these criteria are very rare. Brief experimental surveys of K and Rb under similar pumping conditions did not reveal any additional core-excited laser systems. Spectroscopic searches of this type are difficult since the dominant decay from the upper level of such system is nonradiative. Significant emission on the lasing transition will not occur unless the correct high-gain conditions are produced.

Although the 96.9-nm Cs laser system is rare, there may be other ways to use a traveling-wave photoelectron source to produce neutral XUV lasers. In particular, the requirement that the level to which the ground state is pumped also have a relatively strong XUV laser transition is not necessary. It need only be necessary that the electron pumping rate be large and that the level to be pumped be relatively long lived. A large XUV laser oscillator strength may then be obtained by using a visible laser to transfer population from this long-lived state to some strongly radiating state. It should be noted that detailed knowledge of the core-excited spectroscopy of such a system would be necessary. However, this spectroscopy would be difficult to obtain experimentally since both ejected-electron and photoabsorption spectroscopy would not easily reveal the location of potential long-lifetime intermediate states.

Finally, our studies in Cs have also illustrated the importance of a traveling-wave pumping geometry. The correct traveling-wave excitation is not dependent upon the time with respect to the pump pulse at which the inversion is created since each successive section of the target will be similarly delayed. It is, however, dependent upon the duration of the inversion and on the group velocity of the pulse in the gain media. In high-gain, short-lifetime laser systems, the optimum traveling-wave speed should certainly not be faster than the speed of light in vacuum and may even be less. This fact should play a role in future soft-x-ray laser designs. In particular, the pumping problems associated with K-shell ionization driven soft-x-ray lasers are directly analogous to those faced in this study, i.e., short upper-state lifetimes which are dominated by a nonradiative decay channel [38,39].

[1] C. P. J. Barty, D. A. King, G. Y. Yin, K. H. Hahn, J. E. Field, J. F. Young, and S. E. Harris, Phys. Rev. Lett. **61**, 2201 (1988).

[2] J. K. Spong, J. D. Kmetec, S. C. Wallace, J. F. Young, and S. E. Harris, Phys. Rev. Lett. **58**, 2631 (1987).

[3] J. K. Spong, A. Imamoglu, R. Buffa, and S. E. Harris, Phys. Rev. A **38**, 5617 (1988).

[4] S. E. Harris and J. F. Young, J. Opt. Soc. Am. B **4**, 547 (1987).

[5] S. E. Harris, Opt. Lett. **5**, 1 (1980).

[6] E. J. McGuire and M. A. Duguay, Appl. Opt. **16**, 83 (1977).

[7] H. Egger, T. S. Luk, W. Muller, H. Pummer, and C. K. Rhodes, in *Laser Techniques in the Extreme Ultraviolet, (Boulder, Colorado)*, Proceedings of the Second Topical Meeting on Laser Techniques in the Extreme Ultraviolet, edited by S. E. Harris and T. B. Lucatorto, AIP Conf. Proc. No. 119 (AIP, New York, 1984), p. 64.

[8] W. T. Silfvast and O. R. Wood II, J. Opt. Soc. Am. B **4**, 609 (1987).

[9] H. C. Kapteyn, R. W. Lee, and R. W. Falcone, Phys. Rev. Lett. **57**, 2939 (1986).

[10] D. J. Walker, C. P. J. Barty, G. Y. Yin, J. F. Young, and S. E. Harris, Opt. Lett. **12**, 894 (1987).

[11] J. C. Wang, R. G. Caro, and S. E. Harris, Phys. Rev. Lett. **51**, 767 (1983).

[12] R. G. Caro, J. C. Wang, J. F. Young, and S. E. Harris, Phys. Rev. A **30**, 1407 (1984).

[13] S. J. Benerofe, G.-Y. Yin, C. P. J. Barty, J. F. Young, and S. E. Harris, Phys. Rev. Lett. **66**, 3136 (1991).

[14] G. L. Epstein and J. Reader, J. Opt. Soc. Am. **66**, 590 (1976).

[15] J. Reader, Phys. Rev. A **13**, 507 (1975).

[16] C. J. Sansonetti and K. L. Andrew, J. Opt. Soc. Am. B **3**, 386 (1986).

[17] C. J. Sansonetti, Ph.D. dissertation, Departmetn of Physics, Purdue University, W. Lafayette, IN, 1981.

[18] H. C. Kapteyn, M. M. Murnane, R. W. Falcone, G. Kolbe, and R. W. Lee, Proc. Soc. Photo-Opt. Instrum. Eng. **688**, 54 (1986).

[19] G.-Y. Yin, C. P. J. Barty, D. A. King, D. J. Walker, S. E. Harris, and J. F. Young, Opt. Lett. **12**, 331 (1987).

[20] M. H. Sher, J. J. Macklin, J. F. Young, and S. E. Harris, Opt. Lett. **12**, 891 (1987).

[21] H. K. Chung, J. B. Lee, and T. A. DeTemple, Opt. Commun. **39**, 105 (1981).

[22] E. E. Moore, *Atomic Energy Levels* (U.S. GPO, Washington, D.C., 1971).

[23] R. D. Cowan, *The Theory of Atomic Structure and Spectra* (University of California Press, Berkeley, CA, 1981).

[24] J. P. Connerade, Astrophys. J. **159**, 685 (1970).

[25] V. Pejcev and K. J. Ross, J. Phys. B **10**, 2935 (1977).

[26] A. J. Mendelsohn, C. P. J. Barty, M. H. Sher, J. F. Young, and S. E. Harris, Phys. Rev. A **35**, 2095 (1987).

[27] J. Reader (private communication).

[28] D. Strickland and G. Mourou, Opt. Commun. **56**, 219 (1985).

[29] C. P. J. Barty, Ph.D. dissertation, Department of Applied Physics, Stanford University, Stanford, CA, 1990.

[30] Z. Bor, S. Szatmári and A. Müller, Appl. Phys. B **32**, 101 (1983).

[31] G. L. Linford, E. R. Peressini, W. R. Sooy, and M. L. Spaeth, Appl. Opt. **31**, 379 (1974).

[32] M. H. Sher, Ph.D. dissertation, Department of Applied Physics, Stanford University, Stanford, CA, 1990.

[33] J. D. Kilkenny, P. Bell, R. Hanks, G. Power, R. E. Turner, and J. Wiedwald, Rev. Sci. Instrum. **59**, 1793 (1988).

[34] G. Power and R. Bonner, Proc. Soc. Photo-Opt. Instrum. Eng. **1155**, 439 (1990).

[35] J. Berkowitz, *Photoabsorption, Photoionizatin, and Photoelectron Spectrscopy* (Academic, New York, 1979).

[36] S. E. Harris, Phys. Rev. Lett. **62**, 1033 (1989).

[37] J. Reader, J. Opt. Soc. Am. **73**, 349 (1983).

[38] T. S. Axelrod, Phys. Rev. A **13**, 376 (1976).

[39] H. C. Kapteyn, Ph.D. dissertation, Department of Physics, University of California at Berkeley, Berkeley, CA, 1989.

gold coated
transmission line

microchannel
plate

visible phosphor

fiber bundle
plate

vacuum isolation
o-ring

index matching
grease

imaging system

XUV
photon

energetic
electrons

visible microchannel
plate enhancer

CCD

1 kV, 400 ps gate pulse

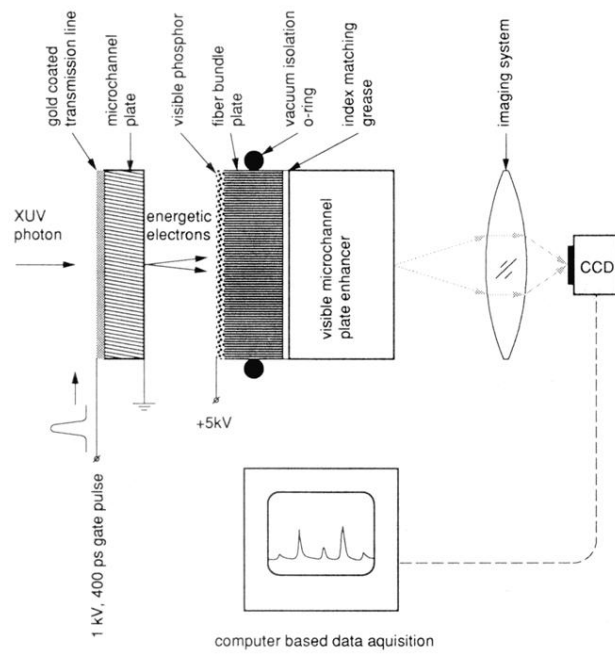+5kV

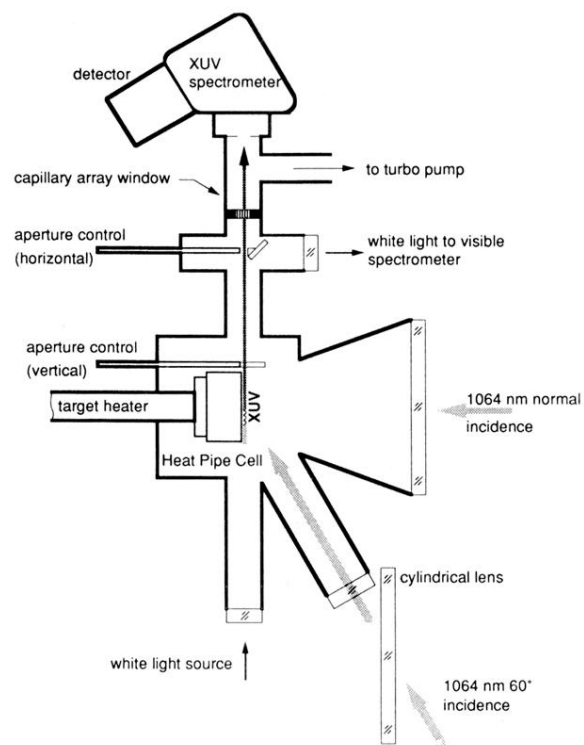computer based data aquisition

FIG. 10. Gated XUV detection system.

FIG. 3. Small-cell experimental arrangement.